Real space models for microstructural evolution

P.-W. Ma, D.R. Mason, I. Rovelli, T.D. Swinburne, S.L. Dudarev

UK Atomic Energy Authority, Oxfordshire, UK

EUROfusion

CCFE is the fusion research arm of the **United Kingdom Atomic Energy Authority.**
This work has been carried out within the framework of the EUROfusion Consortium and has received funding from the Euratom research and training programme 2014-2018 under grant agreement No 633053 and from the RCUK Energy Programme [grant number EP/P012450/1].

CCFE CULHAM CENTRE FOR FUSION ENERGY

Integrated model for DEMO materials

Plasma as a 3D neutron source

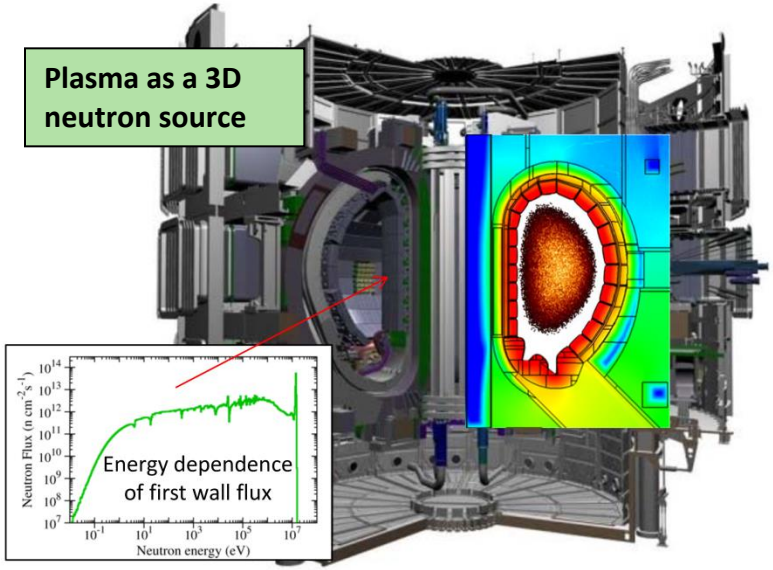

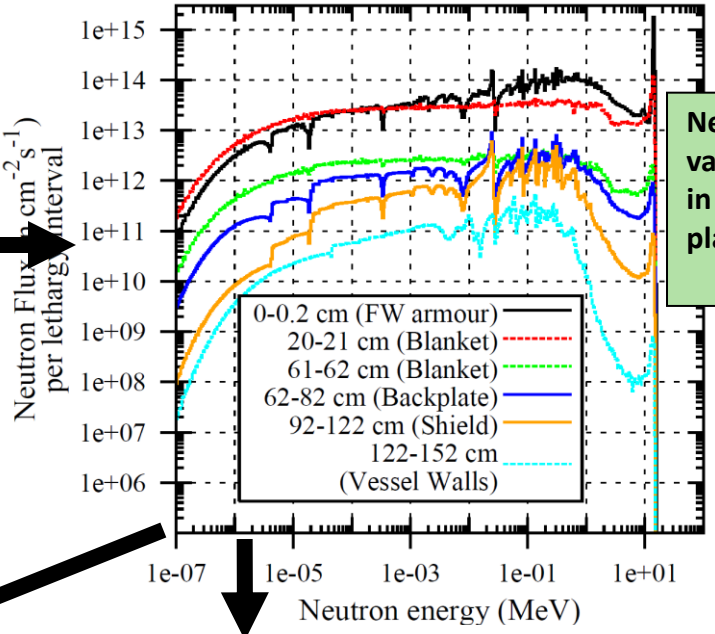

Neutron spectra at various locations in a DEMO power plant

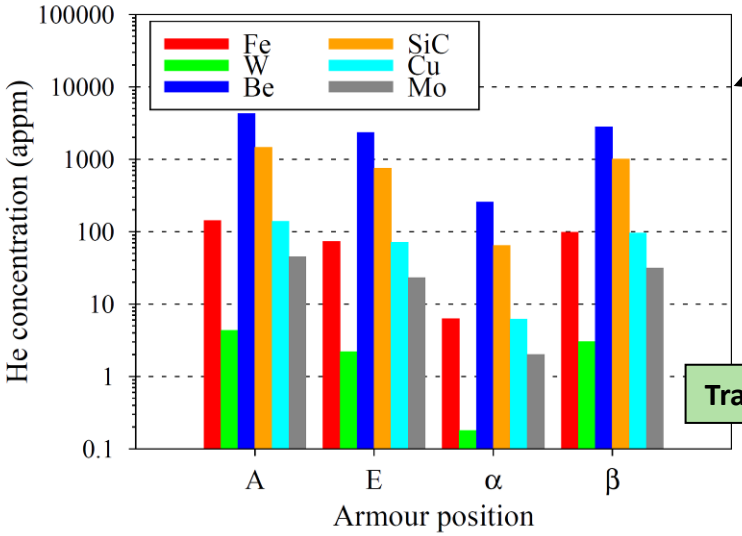

Transmutations

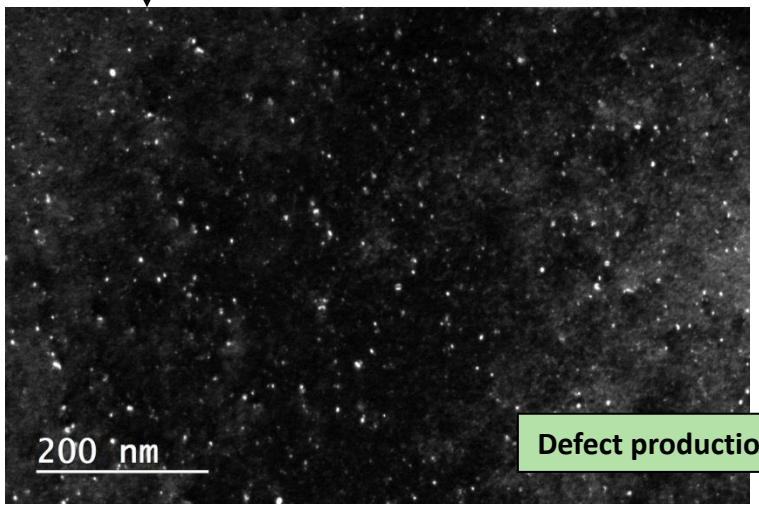

Defect production

M.R. Gilbert *et al*., Nucl. Fusion **52** (2012) 083019; J. Nucl. Mater. **442** (2013) S755; J. Nucl. Mater. **467** (2015) 121

Power density deposited in blanket materials

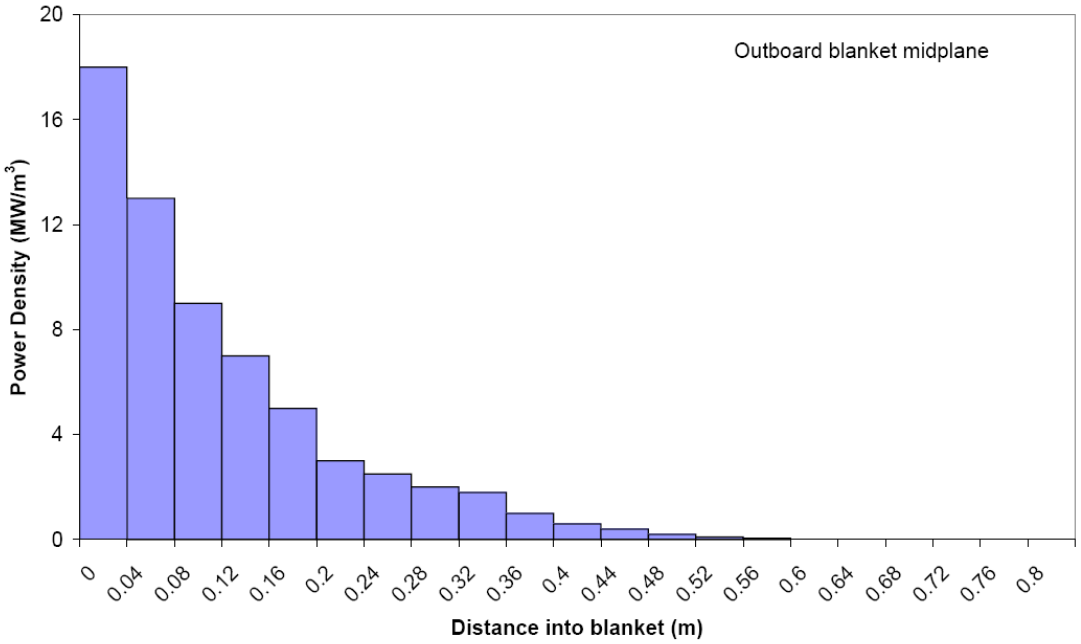

Power density, deposited by neutrons, falls off quickly with distance into the fusion blanket away from the plasma. Most of the energy is deposited in the first 30cm of blanket structure.

S. Sato, K. Maki, Fus. Eng. Design 65 (2003) 501

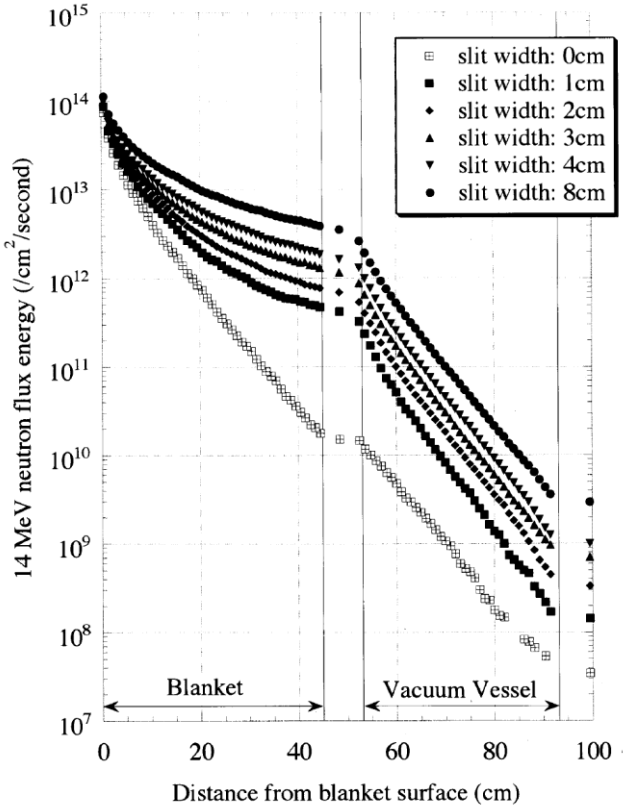

Fig. 2. Distributions of the 14 MeV neutron flux along the slit between the blanket modules under the neutron wall loading of 1 MW am^{-2}, the blanket thickness of 45 cm, the blanket composition of 80% SS and 20% water, the vacuum vessel thickness of 40 cm, and the vacuum vessel shield composition of 60% SS and 40% water.

Energy from neutrons is mostly deposited in the first 10cm of the blanket structure.

Annealing of radiation defects: 1 hour

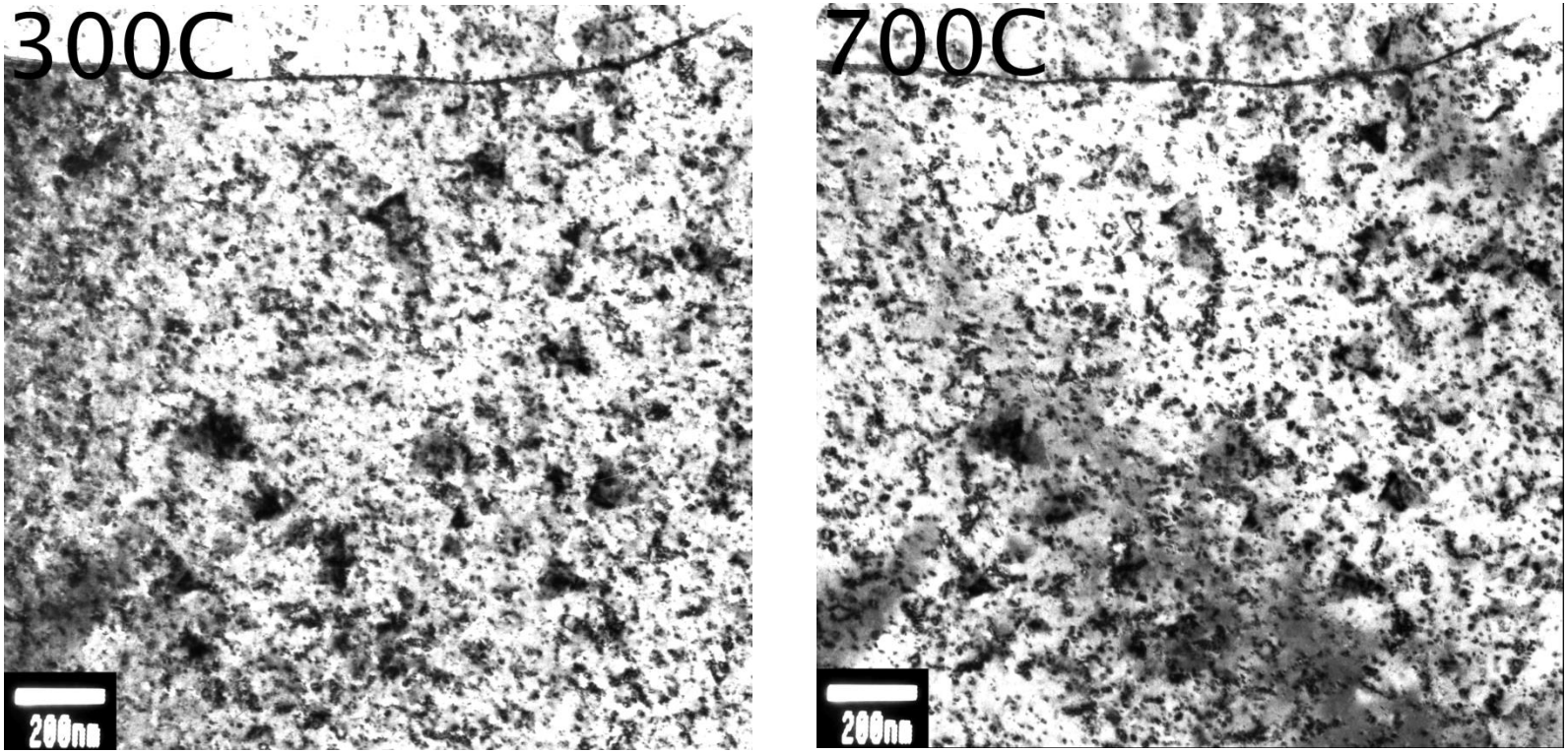

F. Ferroni, X.Yi, K. Arakawa*, et al*., High temperature annealing of ion irradiated (1.5 dpa) tungsten, Acta Mater. **90** (2015) 380.

Annealing of radiation defects: 1 hour

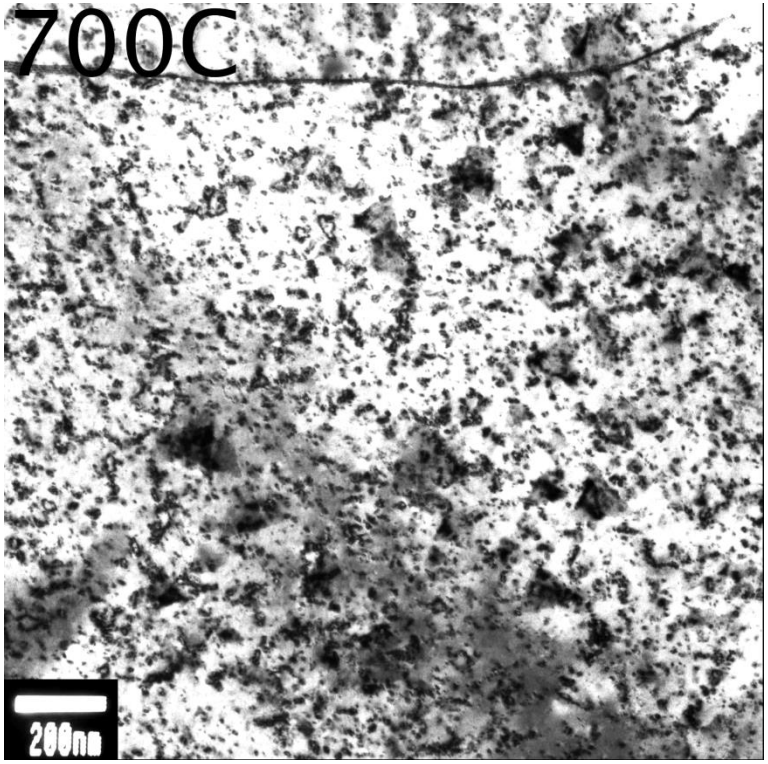

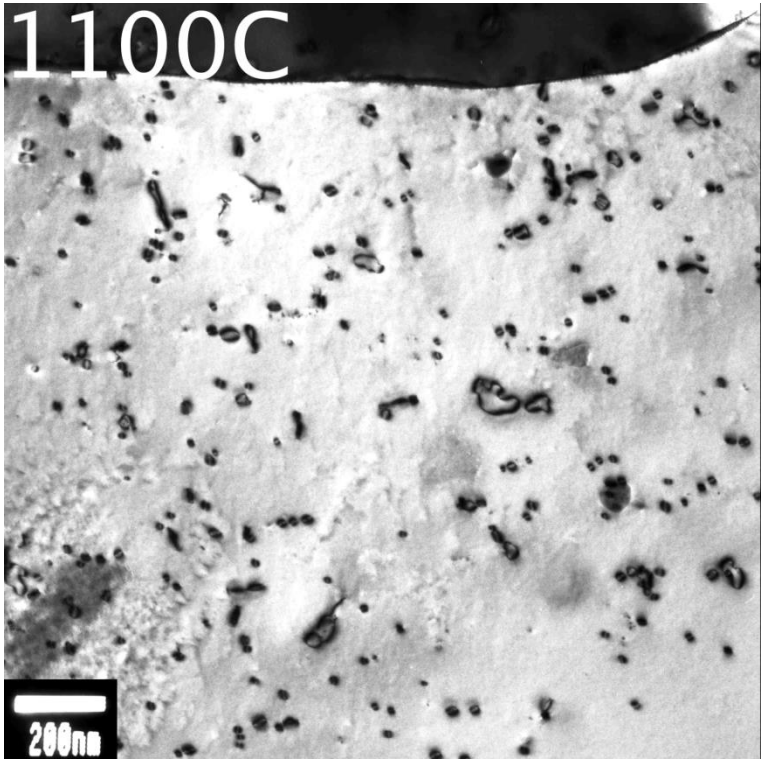

F. Ferroni, X.Yi, K. Arakawa*, et al*., High temperature annealing of ion irradiated (1.5 dpa) tungsten, Acta Mater. **90** (2015) 380.

F. Ferroni, X. Yi, K. Arakawa *et al*., High temperature annealing of ion irradiated (1.5 dpa) tungsten, Acta Mater. **90** (2015) 380. The movie shows the dynamics of recovery of radiation defects at 1100ºC.

Real space models for microstructure

Three-dimensional formulation of dislocation climb

Yejun Gu [a], Yang Xiang [b,*], Siu Sin Quek [c], David J. Srolovitz [d,e]

Journal of the Mechanics and Physics of Solids 83 (2015) 319–337

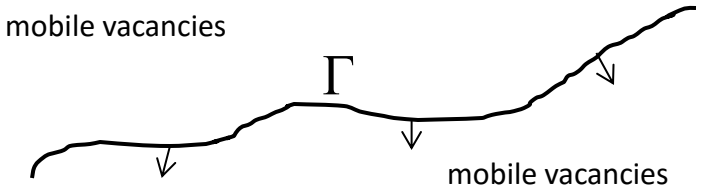

$$\frac{\partial c(\mathbf{x},t)}{\partial t} = -\Omega \nabla J(\mathbf{x},t) - \Omega I(\mathbf{x},t)\delta(\Gamma)$$

$$J(\mathbf{x},t) = -\frac{D_v c(\mathbf{x},t)}{\Omega k_B T} \nabla \mu_v(\mathbf{x},t)$$

Here Γ defines a dislocation line, so that $\int \delta[\Gamma] f(\mathbf{x}) d^3x = \int_\Gamma f(\mathbf{x}) ds.$

In the dilute gas approximation for the chemical potential of vacancies, we arrive at the boundary value problem for a moving dislocation line. A dislocation line moves due to elastic forces acting on it, which stimulate absorption or emission of vacancies:

$$\mu_v(\mathbf{x},t) = k_B T \ln c(\mathbf{x},t);$$

$$D_v \nabla^2 c = b_e v_{cl} \delta(\Gamma)$$

$$c(|\mathbf{x}| \to \infty) = c_\infty$$

Real space models for microstructure

Three-dimensional formulation of dislocation climb

Yejun Gu [a], Yang Xiang [b,*], Siu Sin Quek [c], David J. Srolovitz [d,e]

Journal of the Mechanics and Physics of Solids 83 (2015) 319–337

The central step is the conversion of the boundary value problem into an integral equation

$$c(\mathbf{x}) = \frac{1}{4\pi D_v} \oint_{\Gamma} \frac{\mathbf{b} \cdot (\mathbf{v} \times d\,\mathbf{l}')}{|\mathbf{x} - \mathbf{x}'|} + c_\infty .$$

Assume that a dislocation line forms a closed loop. At large distances from the loop, where $|\mathbf{x}\text{-}\mathbf{x}'| >>$ loop size, this equation acquires a simple form:

$$c(\mathbf{x}) \approx \frac{1}{4\pi D_v |\mathbf{x}|} \oint_{\Gamma} \mathbf{b} \cdot (\mathbf{v} \times d\,\mathbf{l}') + c_\infty .$$

Here

$$\oint_{\Gamma} \mathbf{b} \cdot (\mathbf{v} \times d\,\mathbf{l}') = \frac{d\Omega_{rel}}{dt},$$ and $\Omega_{rel}(t)$ is the volume of the dislocation loop.

Conservation of loop volume during glide

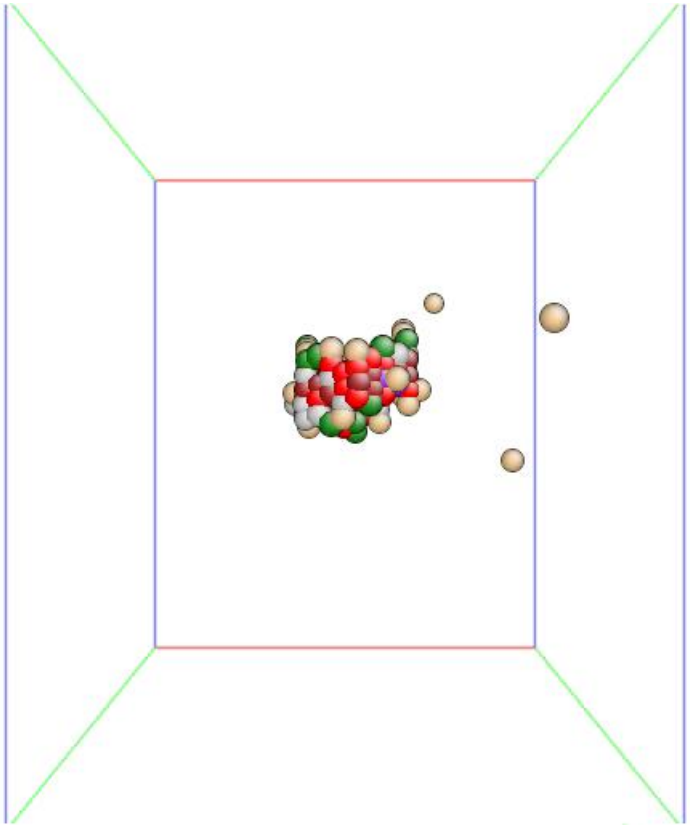

$$\Omega_{rel}(t) = (\mathbf{b} \cdot \mathbf{A}(t))$$

Volume of a loop remains constant during its motion even if the direction and magnitude of the loop vector area changes. Left: simulation of Brownian motion of a dislocation loop. Below: experimental observation of Brownian motion of a dislocation loop by K. Arakawa.

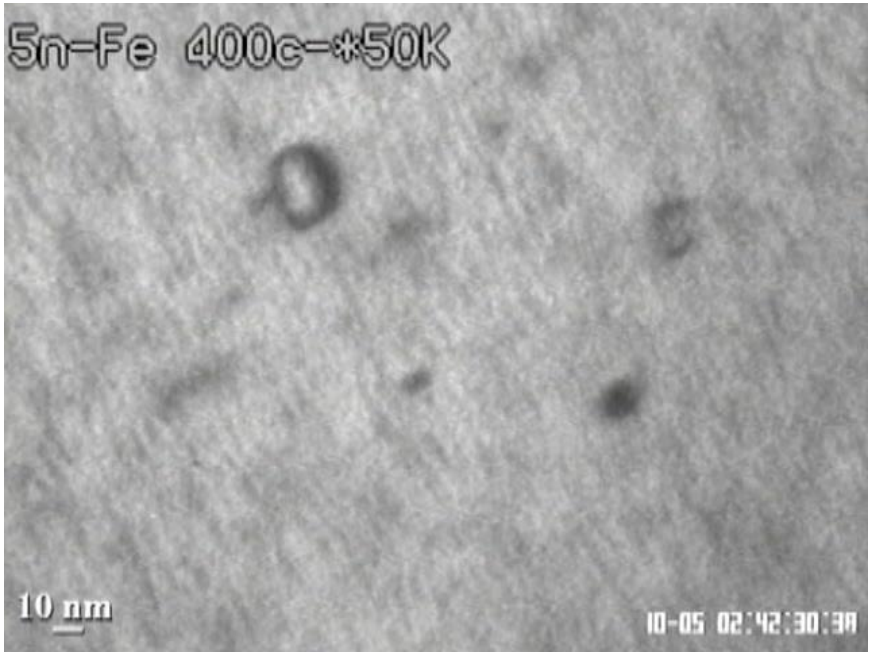

Molecular dynamics simulation of thermal Brownian motion of a ½(111) dislocation loop in iron at 500K, courtesy of M.R. Gilbert.

$$\frac{d\Omega_{rel}}{dt} = \frac{d}{dt}(\mathbf{b} \cdot \mathbf{A}(t)) = 0.$$

Invariant of loop motion.

Real space models for microstructure

The field of vacancies changes adiabatically, following the evolution of dislocation loops (centres of loops are at $\mathbf{x}_i$)

$$c(\mathbf{x}) \approx c_\infty + \frac{1}{4\pi D_v} \sum_i \frac{1}{|\mathbf{x}-\mathbf{x}_i|} \frac{d\Omega^i_{rel}}{dt}.$$

Volume Ω_{rel} of a dislocation loop with Burgers vector $\mathbf{b}$ and area vector $\mathbf{A}$ is given by the scalar product $(\mathbf{b}\cdot\mathbf{A})$ Volume is positive for an interstitial loop and negative for a vacancy loop.

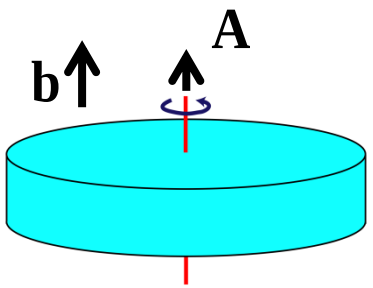

Interstitial loop, $\Omega_{rel} > 0$

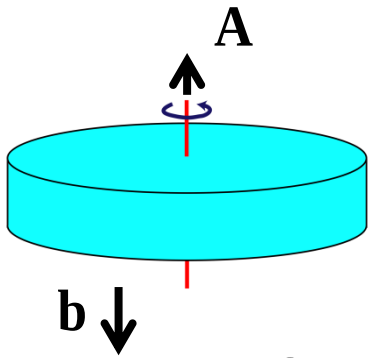

vacancy loop, $\Omega_{rel} < 0$

The above equations for c(**x**) can also be formulated as a set of ODEs for the velocities of nodal points on dislocation lines.

Diffusion to/from surfaces

The computational efficiency of the treatment developed by Y. Gu, Y. Xiang *et al.*, JMPS (2015) is fundamentally due to the use of "free-space" Green's function

$$G_0(\mathbf{x},\mathbf{x}') = -\frac{1}{4\pi D_v |\mathbf{x}-\mathbf{x}'|}.$$

This computational advantage is lost if, in order to take into account the boundary conditions, we attempt to modify these Green's functions. An alternative approach is the Kirchhoff integral approximation, which retains the use of free Green's

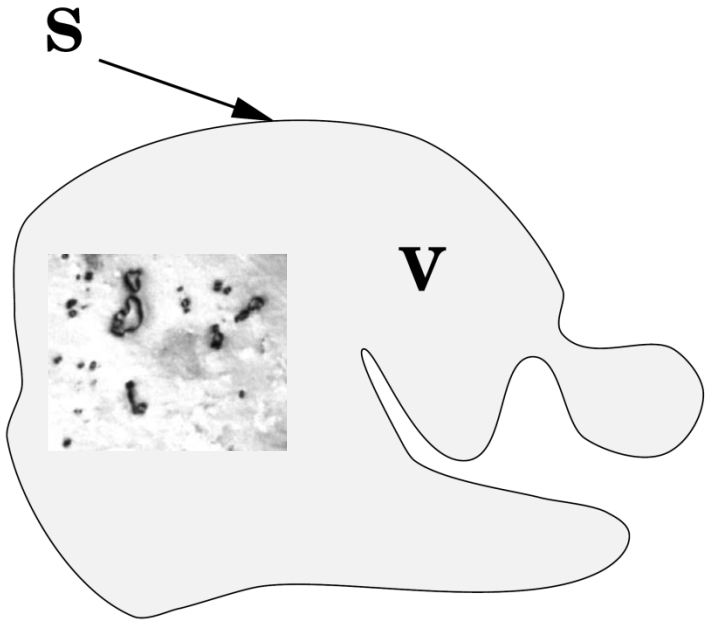

$$\int_V dV\left[\Phi_a(\mathbf{x})\frac{\partial^2\Phi_b(\mathbf{x})}{\partial\mathbf{x}^2} - \Phi_b(\mathbf{x})\frac{\partial^2\Phi_a(\mathbf{x})}{\partial\mathbf{x}^2}\right]$$

$$= \int_S d\mathbf{S}\left[\Phi_a(\mathbf{x})\frac{\partial\Phi_b(\mathbf{x})}{\partial\mathbf{x}} - \Phi_b(\mathbf{x})\frac{\partial\Phi_a(\mathbf{x})}{\partial\mathbf{x}}\right]$$

This formula is known as Green's theorem (G. Green, 1828). It provides the means for treating surfaces and retains the advantages offered by the free Green's function formalism.

Journal of the Mechanics and Physics of Solids 103 (2017) 121–141

Diffusion to/from surfaces

We choose one of the functions in Green's theorem as the vacancy concentration field. The other is free Green's function. This formula below shows that vacancy field can be evaluated everywhere, if c(**x**) and its normal derivatives at surfaces are known.

$$\int_V dV' \left[c(\mathbf{x}') \frac{\partial^2 G_0(\mathbf{x},\mathbf{x}')}{\partial \mathbf{x}'^2} - G_0(\mathbf{x},\mathbf{x}') \frac{\partial^2 c(\mathbf{x}')}{\partial \mathbf{x}'^2} \right] = \int_S dS' \left[c(\mathbf{x}') \left(\mathbf{n} \cdot \frac{\partial G_0(\mathbf{x},\mathbf{x}')}{\partial \mathbf{x}'} \right) - G_0(\mathbf{x},\mathbf{x}') \left(\mathbf{n} \cdot \frac{\partial c(\mathbf{x}')}{\partial \mathbf{x}'} \right) \right]$$

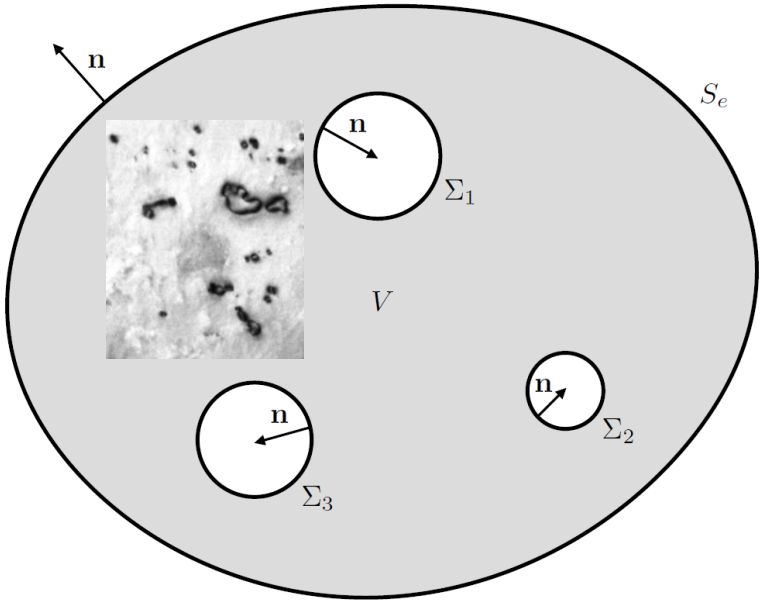

In the right-hand side of this equation, vacancy concentration at a point **x'**, situated at a surface, can be evaluated using the same approach as the one developed for the dislocation loops.

Evaporation of vacancies from dislocation loops is driven by elastic self-stress. In the case of surfaces, it is driven by surface tension.

Arrive at a system of coupled ODEs for the velocities of nodes on dislocation lines and at surfaces. This fully defines the dynamics of diffusion-mediated evolution of loops and cavities/surfaces.

Journal of the Mechanics and Physics of Solids 103 (2017) 121–141

Diffusion to/from surfaces

Equations, describing the vacancy diffusion-mediated evolution of dislocation loops, cavities *and* the external surface, have the form:

$$\omega(\mathbf{x})c(\mathbf{x}) = D_v \int_S dS' \left[c(\mathbf{x}') \left(\mathbf{n} \cdot \frac{\partial G_0(\mathbf{x},\mathbf{x}')}{\partial \mathbf{x}'} \right) - G_0(\mathbf{x},\mathbf{x}') \left(\mathbf{n} \cdot \frac{\partial c(\mathbf{x}')}{\partial \mathbf{x}'} \right) \right]$$

Here $\omega(\mathbf{x}) = 1$ in the bulk, $\omega(\mathbf{x}) = 1/2$ at surfaces (this comes from the integration of a delta-function at the surface) and $\omega(\mathbf{x}) = 0$ in the vacuum. 'Surfaces' also include the toroidal surfaces wrapped around dislocation lines.

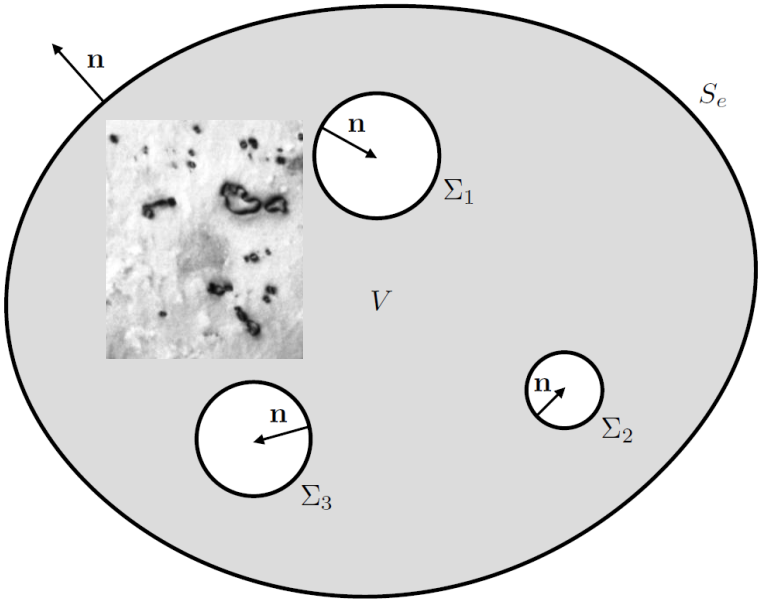

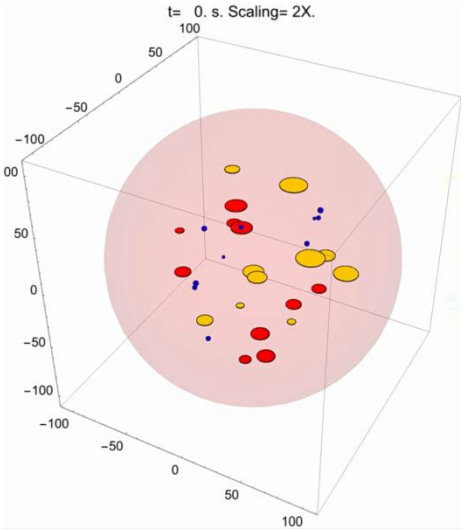

This animation shows evolution of voids, interstitial and vacancy dislocation loops, evolving through the evaporation and exchange of vacancies in tungsten at 1750K.

Journal of the Mechanics and Physics of Solids 103 (2017) 121–141

Applications: evolution timescales

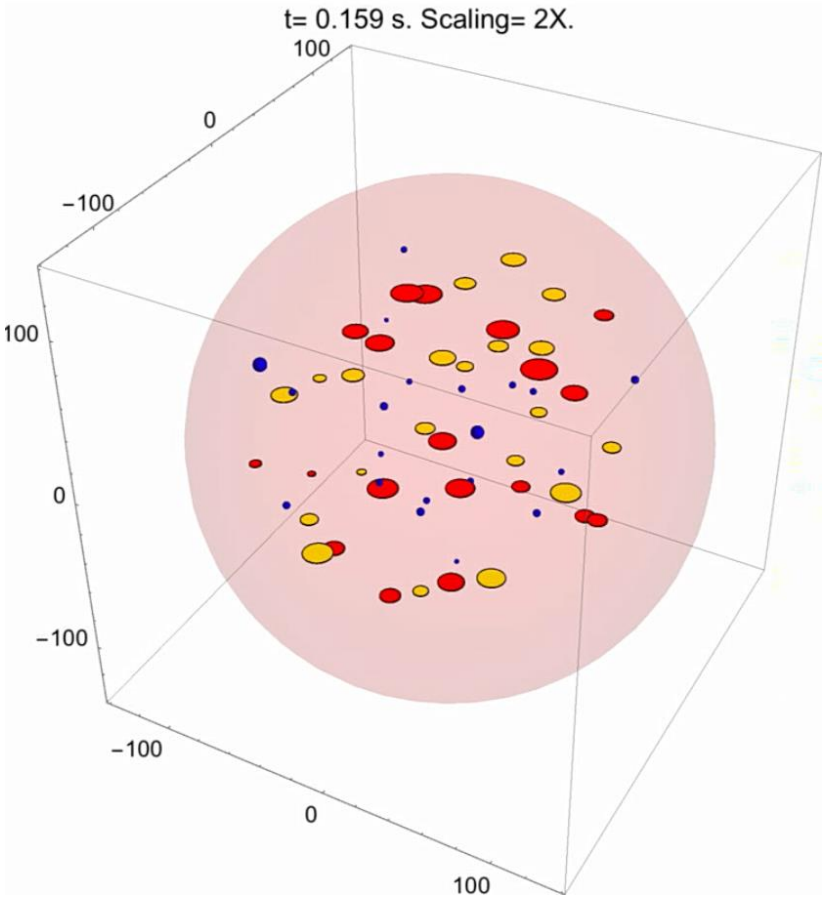

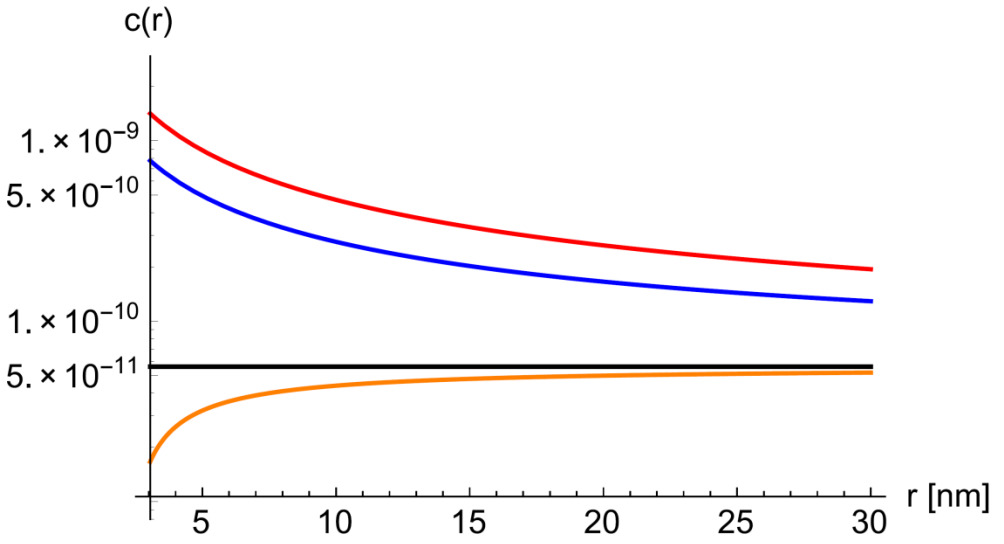

Vacancy concentration profiles plotted as a function of distance from a typical object. Vacancy loops (red) and voids (blue) generate local zones with high concentration of diffusing vacancies, exceeding the background concentration by over two orders of magnitude. Interstitial loops produce local vacancy depleted zones.

Evolution of 20 cavities, 20 interstitial loops (yellow) and 20 vacanc loops (red) randomly distributed with the average number density $5x10^{-6}$ nm^{-3}, in a spherical sample of radius R=142 nm. Objects' radii are initially normally distributed: with the mean of 3.2 nm and standard deviation of 1 nm (loops); with the mean of 1 nm and standard deviation of 0.1 nm (18 smaller cavities); with the mean of 2.2 nm and standard deviation of 0.22 nm (for the two larger cavities).

Journal of the Mechanics and Physics of Solids 103 (2017) 121–141

Elasticity-driven self-climb of dislocations

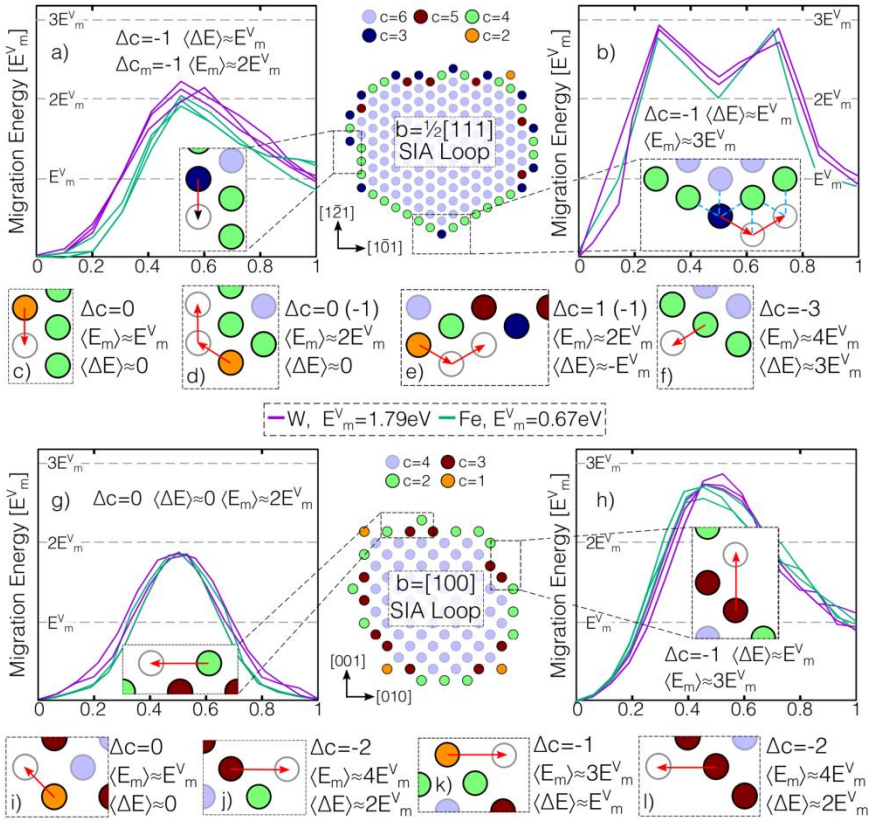

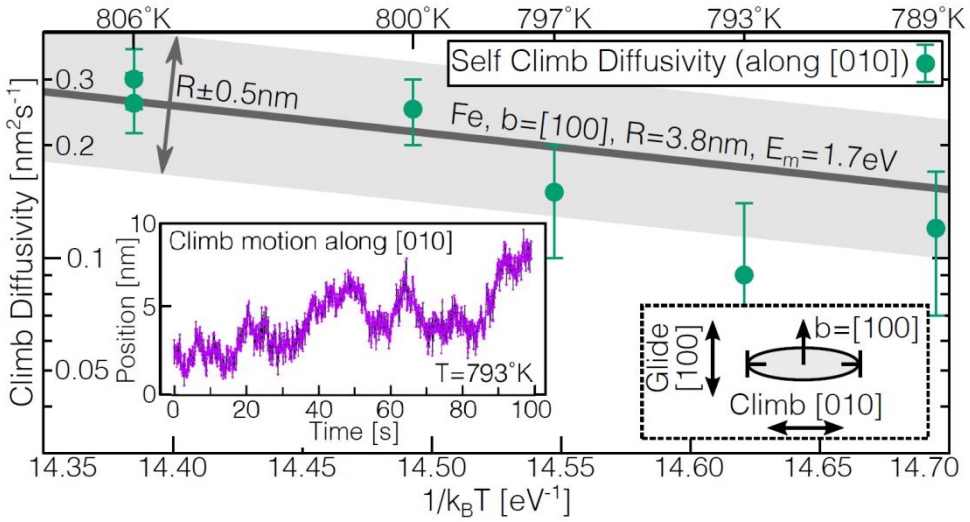

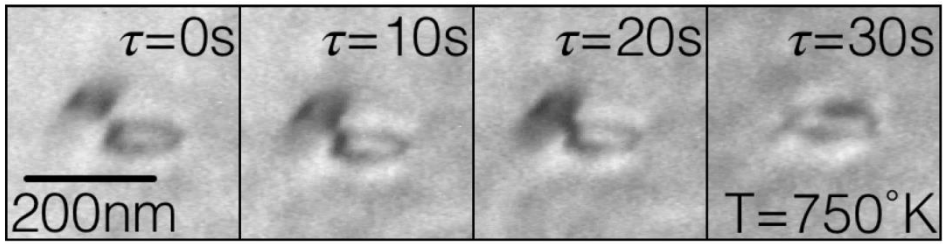

	R_1[nm]	R_2[nm]	d[nm]	T[K]	τ_{exp}[s]	τ_{SC}[s]	τ_{VMC}[s]
Fe	150	30	70	750	30.0	50.2	3.3×10^{7}
Fe	3.5	3.5	7	660	~0.8	1.8	2.7×10^{7}
Fe[§]	~5.	~5.	~10.	725	~6.	2.1	2.7×10^{7}
W[†]	20	20	100	1173	66.5	96.2	2.6×10^{7}
W[†]	100	500*	100	1273	7.	8.6	1.5×10^{5}

Dislocation climb may also occur due to diffusion of atoms around the perimeter of dislocation loops, independent of the vacancy atmosphere. At relatively low temperatures this vacancy-free climb is many orders of magnitude faster than vacancy-diffusion-mediated climb.

T.D. Swinburne *et al.*, Scientific Reports **6** (2016) 30596

Langevin dynamics of interacting defects

3D Langevin dynamics for interacting defects:

$$\frac{dr_i^\alpha}{dt} = -\frac{D_i^{\alpha\beta}}{k_B T}\frac{\partial E}{\partial r_i^\beta} + v_i^\alpha(t), \quad \langle v_i^\alpha(t) v_j^\beta(t')\rangle_T = 2D_i^{\alpha\beta}\delta_{ij}\delta(t-t')$$

- Diffusion coefficients are parameters of the model, related to defect mobilities via the fluctuation-dissipation theorem.
- Interaction between defects is derived from elasticity (isotropic or anisotropic) – this is not a parameter of the model.
- Fluctuating thermal force is an essential ingredient of the model, it is required by the fluctuation-dissipation theorem.

S.L. Dudarev et al., Phys. Rev. B **81**, 224107 (2010)

Langevin dynamics of interacting defects

$$\frac{dr_i^\alpha}{dt} = -\frac{D_i^{\alpha\beta}}{k_B T}\frac{\partial E}{\partial r_i^\beta} + v_i^\alpha(t), \quad \langle v_i^\alpha(t) v_j^\beta(t')\rangle_T = 2D_i^{\alpha\beta}\delta_{ij}\delta(t-t')$$

This set of linked stochastic equations is exactly equivalent to a many-body diffusion equation of the form

$$\frac{\partial P}{\partial t} = \sum_i D_i^{\alpha\beta}\frac{\partial}{\partial r_i^\alpha}\left(\frac{\partial P}{\partial r_i^\beta} + \frac{P}{k_B T}\frac{\partial E}{\partial r_i^\beta}\right); \quad \text{where} \quad P = P(\mathbf{r}_1, \mathbf{r}_2, ..., \mathbf{r}_N, t)$$

The procedure goes beyond the statement of equivalence. The many-body diffusion equation is not solvable. The mapping is similar to mapping a quantum many-body problem of interacting particles onto a set of the Kohn-Sham equations for “independent” quasi-particles.

The Langevin equations can be integrated using algorithms developed for molecular dynamics.

S.L. Dudarev et al., Phys. Rev. B **81**, 224107 (2010)

Strains and stresses produced by defects

$$u_i(\mathbf{r}) = -P_{jk}\frac{\partial}{\partial x_k}G_{ij}(\mathbf{r}); \quad \mathbf{r} = (x_1, x_2, x_3)$$

A formula, central to the treatment of elastic fields, strains and stresses produced by defects. $G_{ij}(r)$ is Green's function of elasticity equations, and P_{ij} is the elastic dipole tensor of a defect.

From the elastic dipole tensor of a defect, it is possible to evaluate its relaxation volume, and compute swelling resulting from the accumulation of defects in a material. There is a beatiful mathematical formula for the relaxation volume of a dislocation loop.

It is also possible to evaluate the energy of interaction beween any two defects

$$E(\mathbf{r}) = P_{ik}^{(1)}P_{jl}^{(2)}\frac{\partial^2}{\partial x_k \partial x_l}G_{ij}(\mathbf{r})$$

Acta Materialia 125 (2017) 425–430

Interaction between crowdion defects

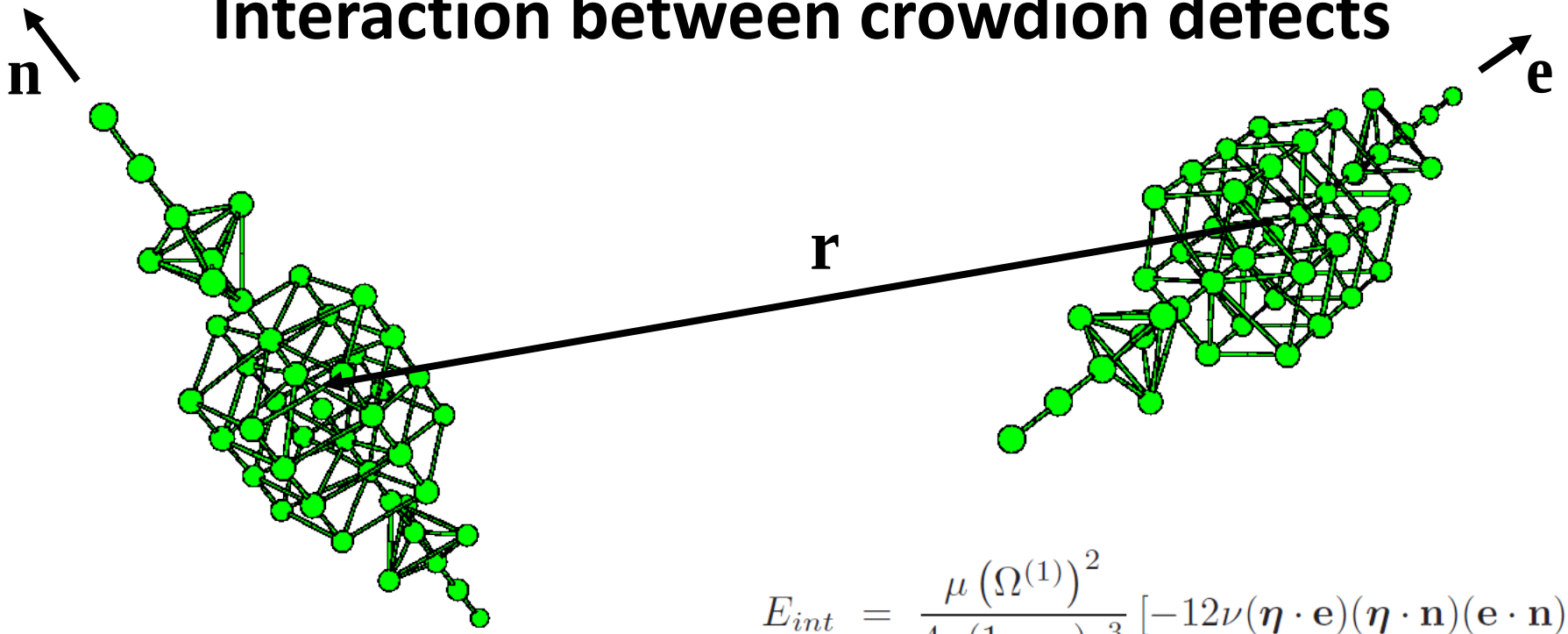

The energy of interaction between the two defects depends on the distance between them, and on their orientation. Similarly to the case of a two small dislocation loops, it is possible to represent this interaction in a closed analytical form.

$$
\begin{aligned}
E_{int} &= \frac{\mu\left(\Omega^{(1)}\right)^2}{4\pi(1-\nu)r^3}\left[-12\nu(\boldsymbol{\eta}\cdot\mathbf{e})(\boldsymbol{\eta}\cdot\mathbf{n})(\mathbf{e}\cdot\mathbf{n})\right. \\
&+ 2(2\nu-1)(\mathbf{e}\cdot\mathbf{n})^2 + 15(\boldsymbol{\eta}\cdot\mathbf{e})^2(\boldsymbol{\eta}\cdot\mathbf{n})^2 \\
&+ \left. 1 - 3(\boldsymbol{\eta}\cdot\mathbf{e})^2 - 3(\boldsymbol{\eta}\cdot\mathbf{n})^2\right] \\
&+ \frac{\mu}{2\pi(1-\nu)r^3}\Omega^{(1)}\left[\nu\Omega^{(1)} + \frac{(1+\nu)}{3}\Omega^{(2)}\right] \\
&\times \left\{\left[3(\boldsymbol{\eta}\cdot\mathbf{e})^2 - 1\right] + \left[3(\boldsymbol{\eta}\cdot\mathbf{n})^2 - 1\right]\right\},
\end{aligned}
$$

Acta Materialia 125 (2017) 425–430

Langevin dynamics of interacting defects

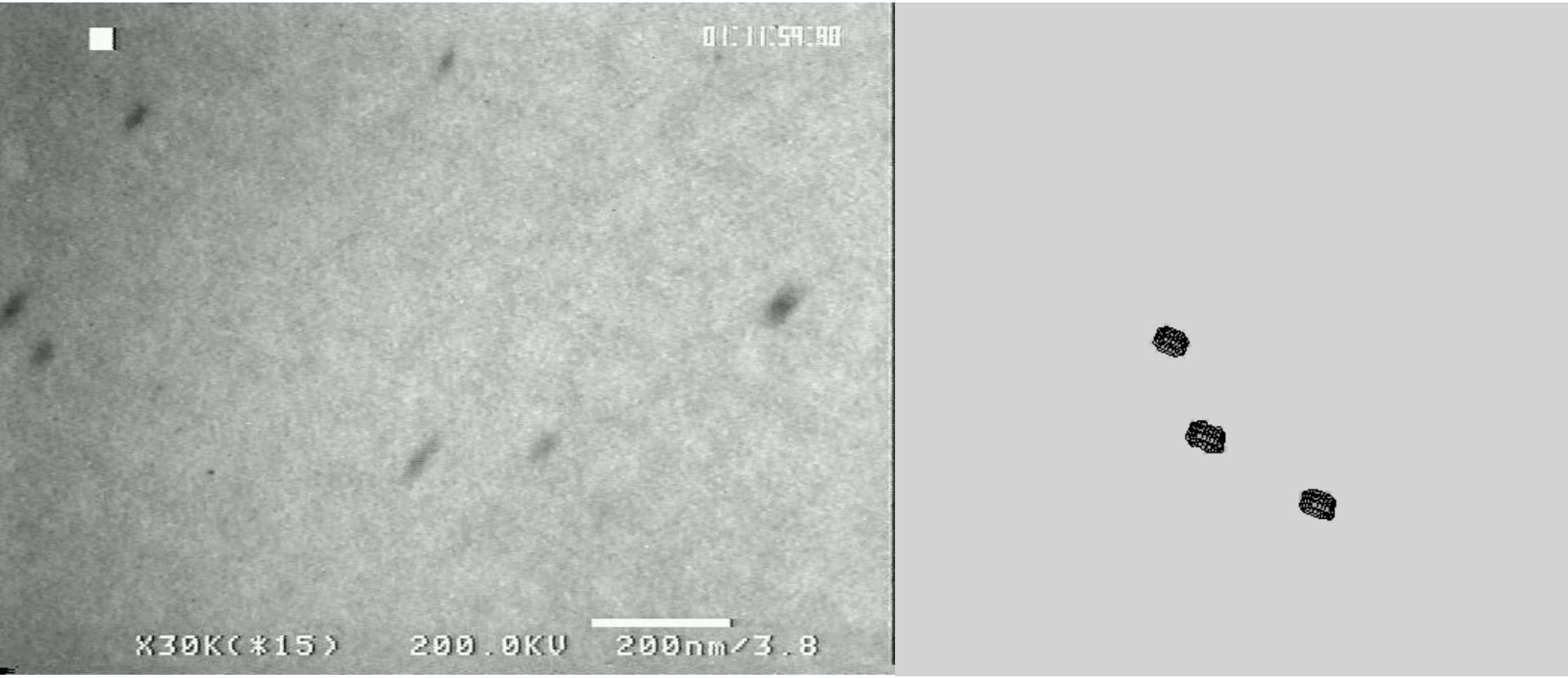

Real-time Langevin simulations of thermally activated migration of interacting loops in pure iron. Left: *in-situ* electron microscope observation of migration of loops (courtesy of Prof. K. Arakawa, Shimane University, Japan), right: a movie derived from simulations. The loop sizes are the same in both cases, interaction laws are derived from isotropic elasticity.

Langevin dynamics of interacting defects

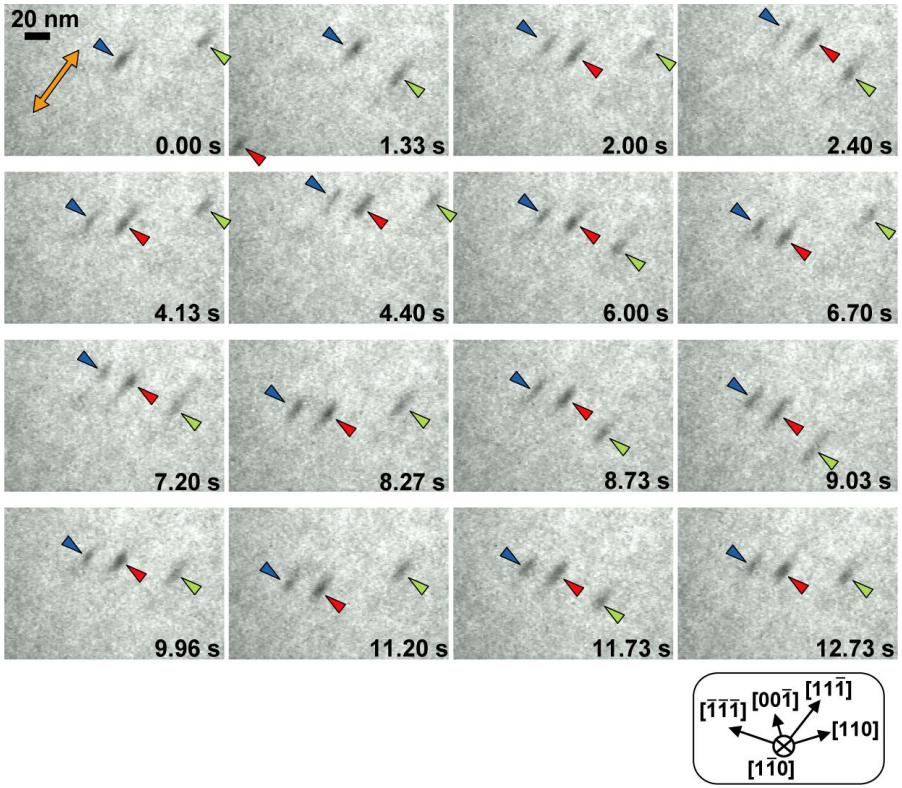

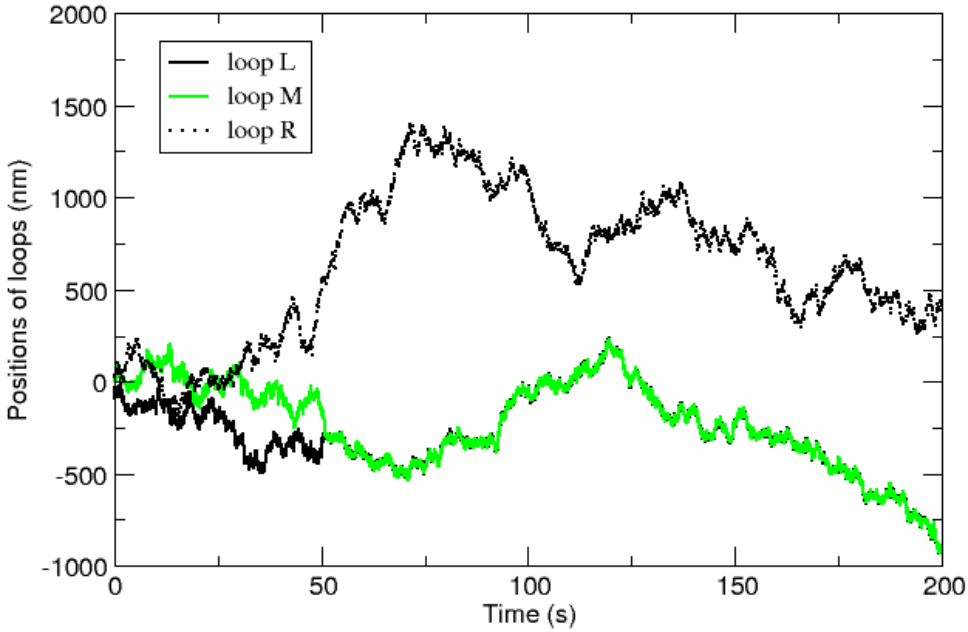

Left: experimentally observed trajectories of three interacting dislocation loops (Arakawa). Right: the simulated trajectories of the three loops. The loops sizes and the distances between the loops match experimental observations.

S.L. Dudarev et al., Phys. Rev. B **81**, 224107 (2010)

Langevin dynamics of interacting defects

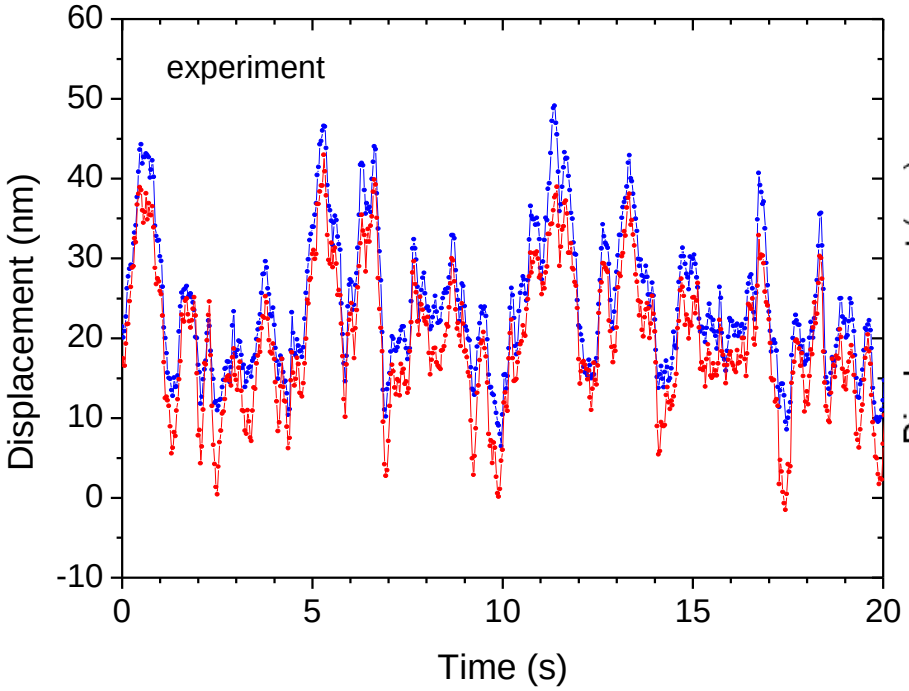

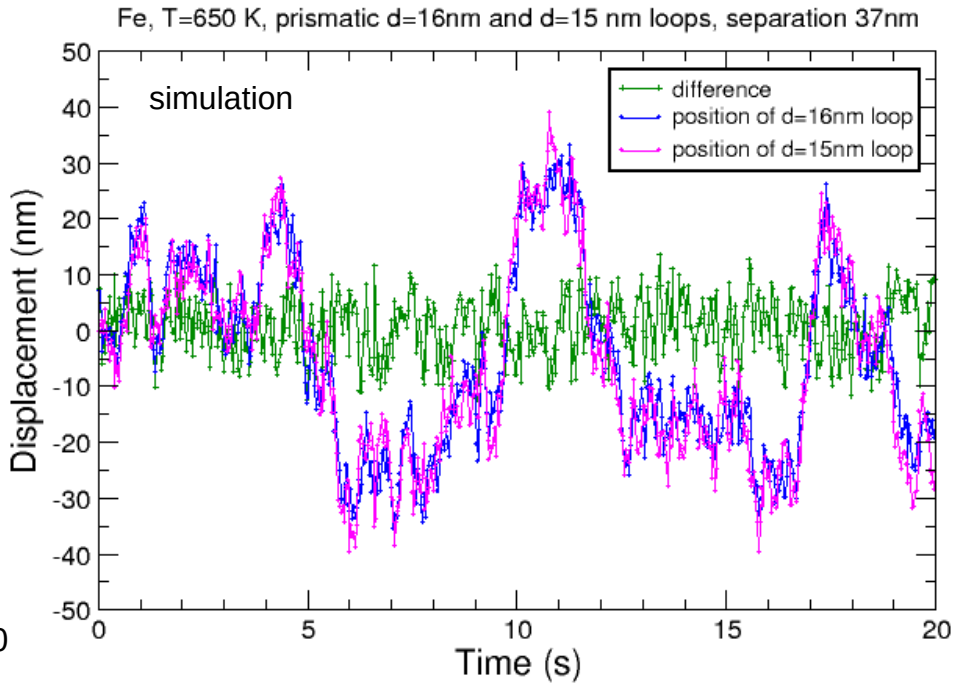

Left: experimentally observed trajectories of two interacting dislocation loops (Arakawa). Right: the simulated trajectories of the two loops. The loops sizes and the distance between the loops match experimental observations.

S.L. Dudarev et al., Phys. Rev. B **81**, 224107 (2010)

Langevin dynamics of interacting defects

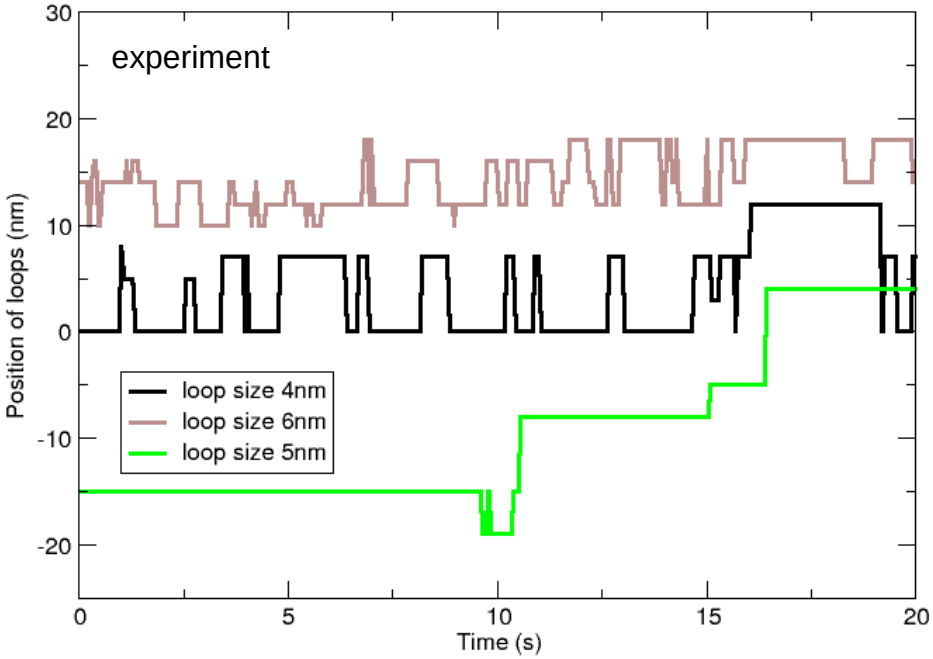

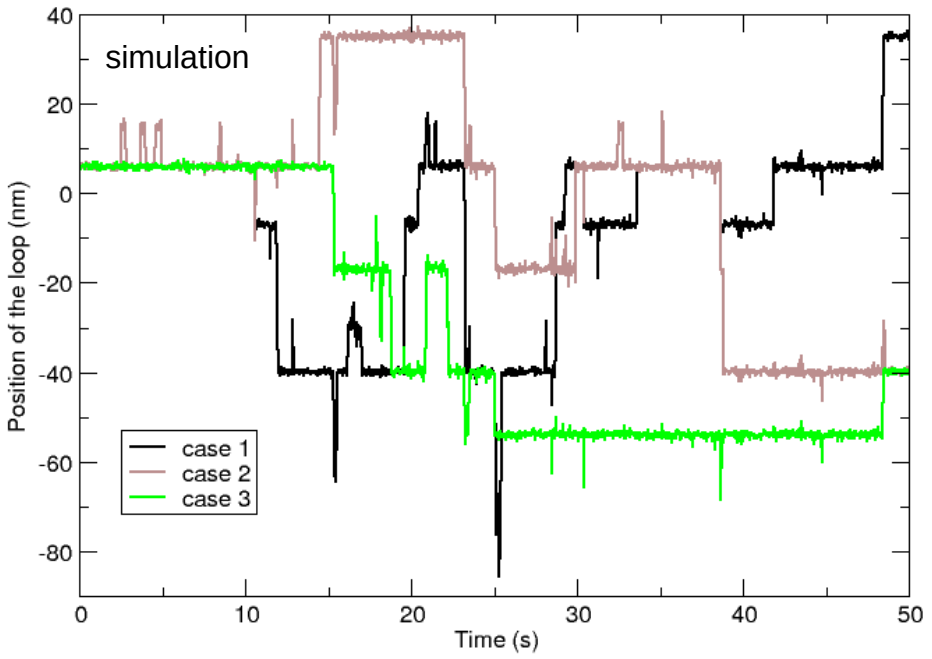

Left: experimentally observed trajectories of loops in ion-irradiated iron (Yao and Jenkins). Right: trajectories of motion simulated using Langevin dynamics, taking into account interaction with the “invisible” vacancy clusters. Loops sizes match those observed experimentally. Note that characteristic ~10 s timescales characterising the motion of defects observed in experiment.

S.L. Dudarev et al., Phys. Rev. B **81**, 224107 (2010)

Relaxation volume of a dislocation loop

$$P_{ij} = \mu \left[(b_i A_j + A_i b_j) + \frac{2\nu}{1-2\nu} (\boldsymbol{b} \cdot \boldsymbol{A}) \delta_{ij} \right].$$

where

$$\mathbf{A} = \frac{1}{2} \oint (\mathbf{r} \times d\mathbf{l})$$

is the vector area of the loop, and **b** is the Burgers vector. The trace of a dipole tensor is proportional to the relaxation volume of the loop

$$\mathrm{Tr} P_{ij} = 2\mu \Omega_{rel} \frac{1+\nu}{1-2\nu}.$$

A simple calculations shows that the elastic relaxation volume of a dislocation loop equals the product of its Burgers vector and its area

$$\Omega_{rel} = (\mathbf{b} \cdot \mathbf{A}) = \frac{1}{2} \oint \mathbf{b} \cdot (\mathbf{r} \times d\mathbf{l})$$

Acta Materialia 125 (2017) 425–430

Is a crowdion an infinitesimally small loop?

To answer the question, we have computed P_{ij} of a crowdion using DFT, and investigated whether the symmetry of the tensor is the same or different from that of an infinitesimal loop.

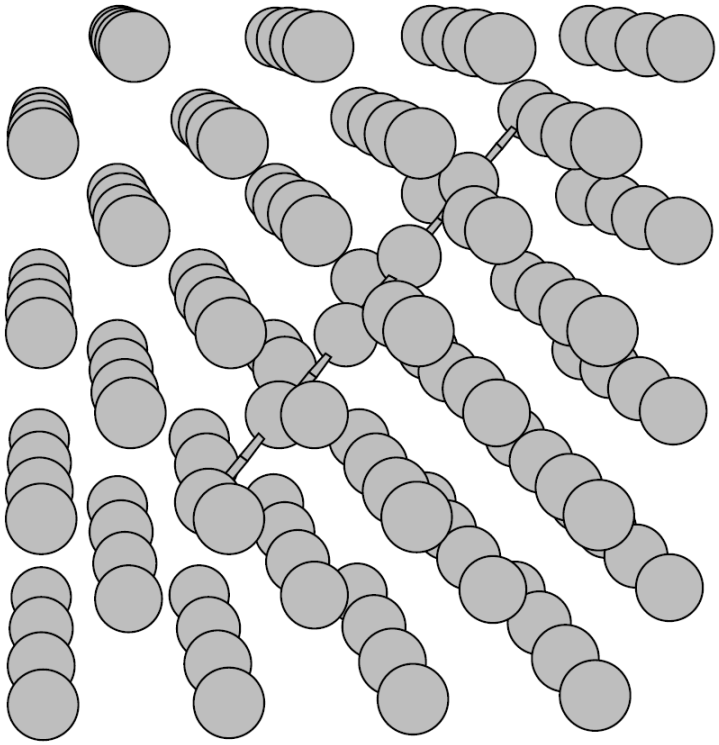

$$P_{ij} = \begin{pmatrix} 53.84 & 13.23 & 13.23 \\ 13.23 & 53.84 & 13.23 \\ 13.23 & 13.23 & 53.84 \end{pmatrix} eV$$

Since tungsten is elastically isotropic, had the crowdion been a small dislocation loop, its dipole tensors should have had the form (of that of an infinitesimal loop)

$$P_{ij} = 2\mu bA\left(n_i n_j + \frac{\nu}{1-2\nu}\delta_{ij} \right)$$

where **n** is a unit vector in the [111] direction.

<u>BUT this form does not fit the DFT data</u>.

Is a crowdion an infinitesimally small loop?

Further analysis shows that in order to parameterise the elastic dipole tensor of a crowdion, <u>two</u> independent parameters are required.

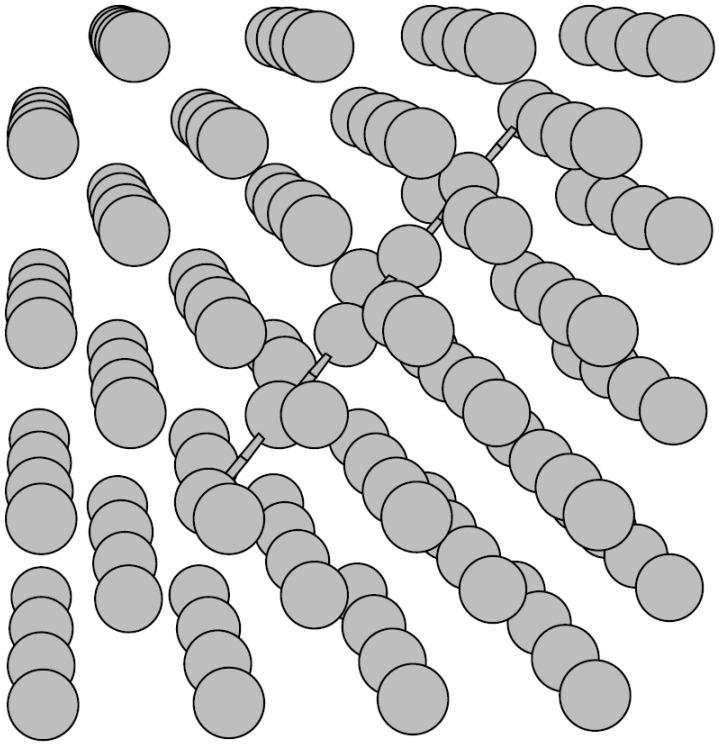

$$P_{ij} = \begin{pmatrix} 53.84 & 13.23 & 13.23 \\ 13.23 & 53.84 & 13.23 \\ 13.23 & 13.23 & 53.84 \end{pmatrix} eV$$

$$P_{ij} = C_{ijkl}\left(\Omega^{(1)} n_i n_j + \frac{\Omega^{(2)}}{3}\delta_{ij}\right)$$

where the sum of these two parameters equals the relaxation volume of the crowdion

$$\Omega_{rel} = \Omega^{(1)} + \Omega^{(2)}$$

<u>This shows that a crowdion is NOT a small dislocation loop.</u>

Parameterization of dipole tensors

	Ω_0	$\Omega^{(1)}$	$\Omega^{(2)}$	Ω_{rel}	Ω_{rel}/Ω_0
W	15.61	20.23	5.84	26.07	1.67
	15.61	20.48	5.55	26.02	1.67
Mo	15.61	17.38	5.29	22.67	1.45
	15.61	17.15	5.51	22.66	1.45
Ta	17.62	19.46	7.01	26.47	1.50
	17.62	17.77	8.46	26.23	1.49
Nb	17.68	30.46	-3.24	27.22	1.54
	17.68	20.57	6.18	26.75	1.51
V	12.91	-1.24	18.17	16.92	1.31
	12.91	-1.37	15.79	14.42	1.12

TABLE V: Equilibrium atomic volume $\Omega_0 = a_0^3/2$, parameters $\Omega^{(1)}$ and $\Omega^{(2)}$ of elastic dipole tensor of a defect (17), the total elastic relaxation volume of the defect, and the same quantity expressed as a fraction of equilibrium atomic volume. All the dimensional values are given in cubic Angstrom units. The first row for each metal shows values computed using the zero strain method, the second row gives values computed using the zero stress method. The elastic relaxation volume of a self-interstitial defect in tungsten given in the table agrees almost exactly with the value found earlier in Ref. 36.

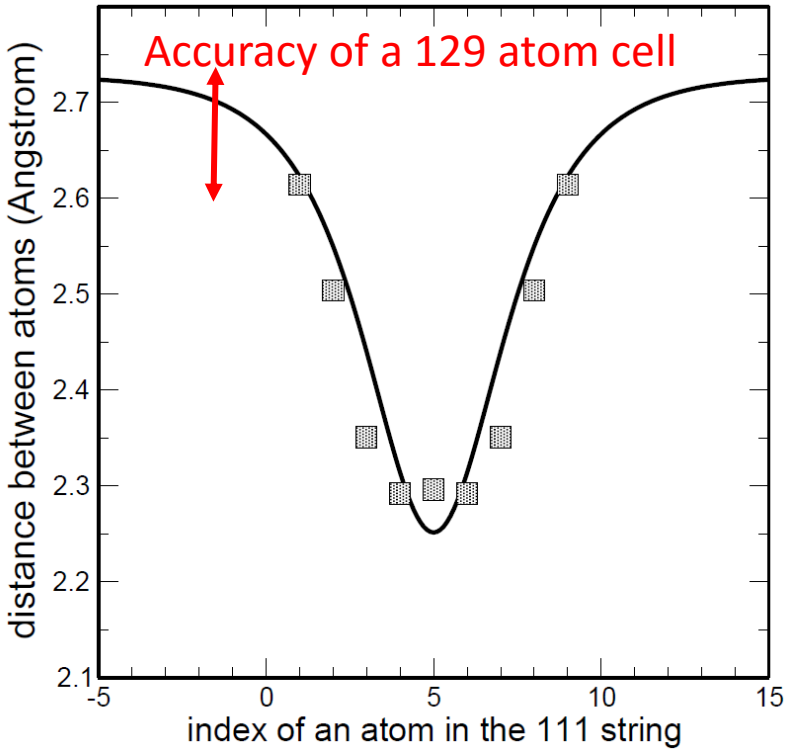

Surprisingly, we find that a 129 atom cell, often used for computing energies of defects, only delivers ~5% accuracy in dipole tensor evaluation.

For a vacancy, $\Omega_{rel}/\Omega_0 = -0.37$

F. Hofmann *et al.*, Acta Mater. **89** (2015) 352

Computer Physics Communications 207 (2016) 350–361

Contents lists available at ScienceDirect

Computer Physics Communications

journal homepage: www.elsevier.com/locate/cpc

SPILADY: A parallel CPU and GPU code for spin–lattice magnetic molecular dynamics simulations☆

Pui-Wai Ma [a,*], S.L. Dudarev [a], C.H. Woo [b]

[a] Culham Centre for Fusion Energy, UK Atomic Energy Authority, Culham Science Centre, Abingdon, Oxfordshire, OX14 3DB, United Kingdom

[b] Department of Physics and Materials Sciences, The City University of Hong Kong, Hong Kong Special Administrative Region

- Full code is available to download from the journal webpage or the CCFE website http://spilady.ccfe.ac.uk
- Time evolution of spins and atoms. In the absence of magnetism, spin-lattice dynamics is equivalent to molecular dynamics.
- Treats the effect of non-collinear magnetism on interatomic forces.

Applications

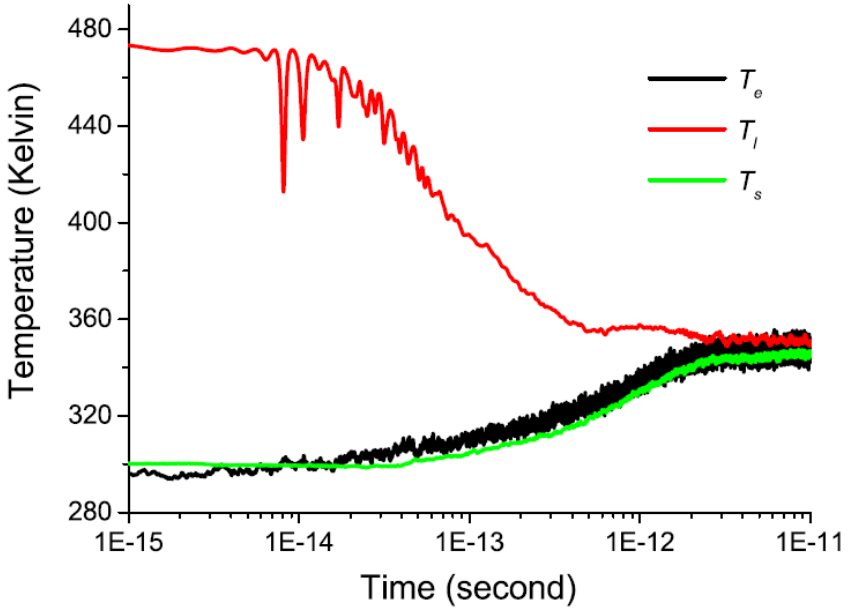

- Variation of lattice T_l, spin T_s and electron T_e temperatures in a collision cascade simulation.
- Simulation was performed using a bcc Fe supercell containing ~220000 atoms.
- The kinetic energy of the primary-knock-on atom (PKA) is 5 keV, initially the lattice is at 300K.

P.-W. Ma, S.L. Dudarev, C. H. Woo, Phys. Rev. B**85** (2012) 184301

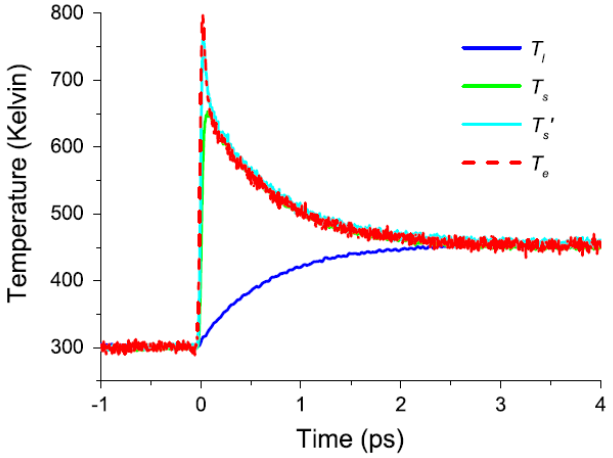

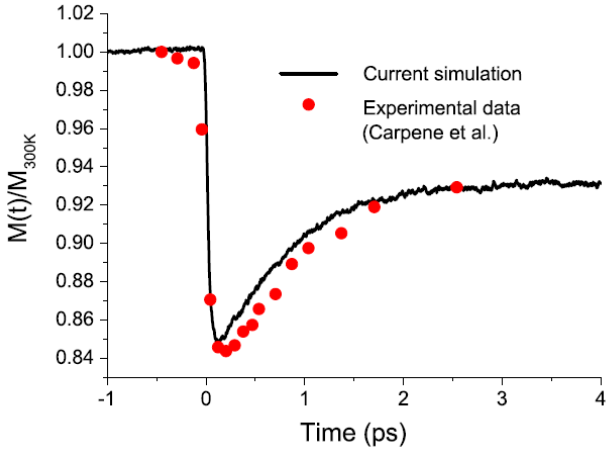

- Laser pulse at t=0.
- Variation of temperatures as functions of time
- Dynamics of demagnetization and recovery in Fe

BCC-FCC-BCC phase transitions in Fe

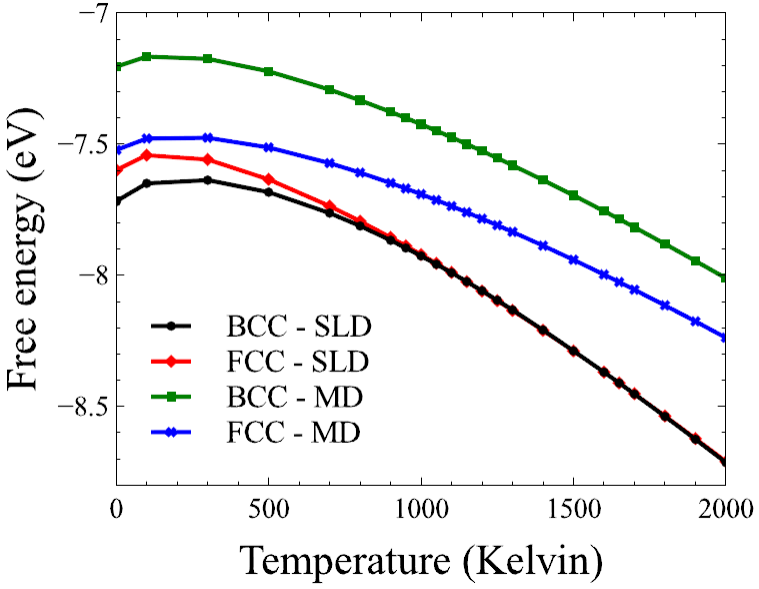

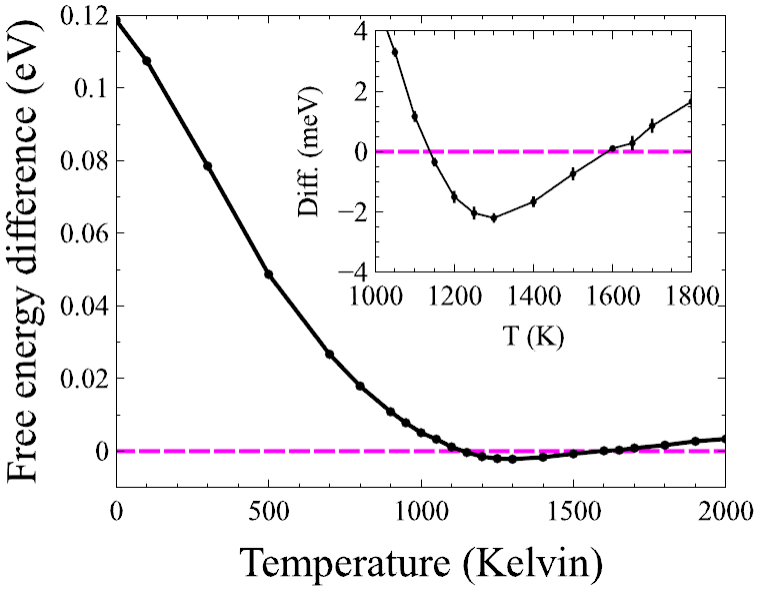

- The maximum bcc-fcc free energy difference over the bcc-fcc-bcc phase transition temperature interval is 2meV per atom.
- The case looks hopeful: similarly to how molecular dynamics has evolved into a predictive tool, spin-lattice dynamics is evolving into an accurate simulation method, capable of modelling dynamic processes at meV/atom level of accuracy.

P.-W. Ma, S.L. Dudarev, J.S. Wrobel , Phys. Rev. B**96** (2017) 094418